Research Article

Vladislav A. Chistyakov, Viktar S. Asadchy, Shanhui Fan, Andrea Alù and Alex Krasnok*

Tunable magnetless optical isolation with twisted Weyl semimetals

https://doi.org/10.1515/nanoph-2023-0241
Received April 18, 2023; accepted June 26, 2023;
published online July 12, 2023

Abstract: Weyl semimetals hold great promise in revolutionizing nonreciprocal optical components due to their unique topological properties. By exhibiting nonreciprocal magneto-optical effects without necessitating an external magnetic field, these materials offer remarkable miniaturization opportunities and reduced energy consumption. However, their intrinsic topological robustness poses a challenge for applications demanding tunability. In this work, we introduce an innovative approach to enhance the tunability of their response, utilizing multilayered configurations of twisted anisotropic Weyl semimetals. Our design enables controlled and reversible isolation by adjusting the twist angle between the anisotropic layers. When implemented in the Faraday geometry within the mid-IR frequency range, our design delivers impressive isolation, exceeding 50 dB, while maintaining a minimal insertion loss of just 0.33 dB. Moreover, the in-plane anisotropy of Weyl semimetals eliminates one or both polarizers of conventional isolator geometry, significantly reducing the overall dimensions. These results set the stage for creating highly adaptable, ultra-compact optical isolators that can propel the fields of integrated photonics and quantum technology applications to new heights.

Keywords: optical isolation; tunable; twisted anisotropic Weyl semimetal; Weyl semimetals

***Corresponding author: Alex Krasnok**, Department of Electrical and Computer Engineering, Florida International University, Miami, FL 33174, USA, E-mail: akrasnok@fiu.edu. https://orcid.org/0000-0001-7419-781X
Vladislav A. Chistyakov, Saint-Petersburg, 191002, Russia, E-mail: v.chistyakov@metalab.ifmo.ru
Viktar S. Asadchy, Department of Electronics and Nanoengineering, Aalto University, 02150, Espoo, Finland, E-mail: viktar.asadchy@aalto.fi. https://orcid.org/0000-0002-9840-4737
Shanhui Fan, Ginzton Laboratory and Department of Electrical Engineering, Stanford University, Stanford, CA, 94305, USA, E-mail: shanhui@stanford.edu
Andrea Alù, Photonics Initiative, Advanced Science Research Center, City University of New York, New York, NY, USA, E-mail: aalu@gc.cuny.edu

1 Introduction

Weyl semimetals (WSs) represent a fascinating 3D topological phase of matter, characterized by low-energy excitations that follow the Weyl equation. These materials contain even numbers of Weyl nodes within their energy band structure, which carry quantized topological charges [1–12]. Quasiparticles near these nodes resemble Weyl fermions in high-energy physics, displaying linear dispersion and distinct chirality. Acting as monopoles of Berry curvature, Weyl nodes remain stable under perturbations. WSs arise from Dirac cone states when either inversion (P) or time-reversal (T) symmetry is broken, and their resilience arises since a Weyl node cannot be eliminated unless through annihilation with another Weyl node with opposite chirality [13]. Both electronic WSs and their photonic analogues have been experimentally verified, demonstrating unique optical properties such as the anomalous Hall effect, chiral magnetic effect, and giant magneto-optical Faraday/Kerr effects [9, 10, 14–21]. Recently, surface plasmons have been demonstrated in Weyl semimetals [22]. Unlike metals, Weyl semimetals can support a magnetoplasmon mode with additional longitudinal field dependence, thus expanding the scope and potential applications of these fascinating materials. These properties give rise to various nonreciprocal phenomena, including nonreciprocal wave transfer, surface plasmons, and thermal emitters, making WSs valuable for fundamental research and practical applications [23–27].

The nonreciprocal light transfer is crucial in photonics [28–30] and quantum technologies [31, 32]. In photonics, isolators are indispensable for creating unidirectional optical circuits, reducing reflections, and eliminating multipath interference in communication channels [33, 34]. Similarly, in quantum technology, isolators play a vital role in safeguarding quantum circuits from noise during readout. Nonreciprocal components primarily rely on the magneto-optical effect found in ferrite materials [33, 35, 36]. Unfortunately, these components are bulky, minimally tunable, and incompatible with planar technologies such as integrated photonics and transmission-line quantum circuits. Alternative approaches, including two-dimensional magnetic materials [37] and time modulation [38], have been explored

extensively in recent years. However, they still encounter tunability, bandwidth, and energy consumption limitations. Recent studies have shown that large optical isolation can be achieved by designing photonic structures based on Weyl semimetals [23, 27, 39, 40]. The strong nonreciprocity in these materials arises from the anomalous Hall effect caused by Weyl node separation [27, 41, 42]. This mechanism differs fundamentally from the cyclotron mechanism in magneto-optical materials, and it does not necessitate an external magnetic field or static magnetization. Nonetheless, the inherent topological properties of these materials present challenges for practical applications that demand tunability.

In this work, we propose a novel approach to tunable optical isolation that utilizes multilayered structures with twisted optically anisotropic bias-free Weyl semimetals. The in-plane anisotropy can be either intrinsic [43, 44], or artificially introduced by surface corrugation on the WS surface. Our approach enables highly efficient tuning of both direction and value of isolation by relative rotation of WSs layers. Moreover, in-plane anisotropy eliminates the need for one or both polarizers, significantly simplifying and downsizing the entire structure. Implemented within the Faraday geometry in the mid-IR frequency range, our design comprises two anisotropic WS layers separated by a dielectric medium. This configuration achieves exceptional isolation performance, surpassing 50 dB while maintaining an ultra-low insertion loss of just 0.33 dB.

2 Results and discussion

Figure 1(a) demonstrates a design that leverages the Faraday geometry. This setup incorporates a three-layer isolator structure composed of two layers of WSs separated by a dielectric with $\epsilon_{\text{diel}} = 5$, and two linear polarizers angled at 45°. The dielectric layer supports a Fabry–Perot resonance, with an electric field mainly concentrated in this layer. This strategic arrangement effectively suppresses the losses incurred in WSs, thus increasing the overall efficiency of the setup. In the spectral range of interest, we have a wide variety of virtually lossless materials of such permittivity, including chalcogenide glasses (e.g., As_2Se_3, As_2S_3), titanium dioxide (TiO_2), and silicon nitride (Si_3N_4).

Polarizers are essential components in optical isolators. The input polarizer ensures the incoming light is linearly polarized in a specific orientation. The Faraday rotator, in our case, the three-layer structure, rotates the plane of polarization by 45° when the light passes through it. The output polarizer is oriented to allow light with the rotated polarization to pass through. When light attempts to travel in the reverse direction, it first passes through the output polarizer, which does not change its polarization. However, when it reaches the Faraday rotator, the polarization is rotated by another 45°. This results in a total rotation of 90° compared to the original forward-traveling light. Since the input polarizer is oriented to block this rotated polarization, the light cannot pass

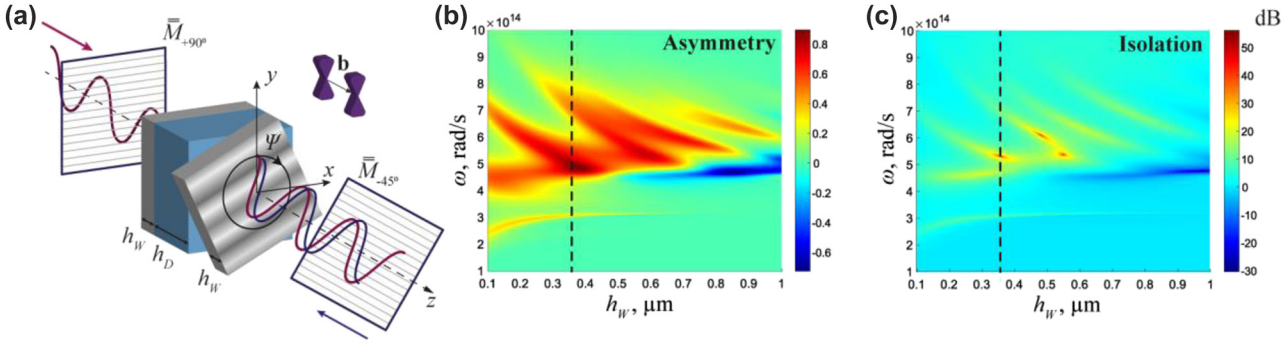

Figure 1: Faraday isolator with twisted Weyl semimetals. (a) Geometry of a Faraday isolator based on a dielectric ($\epsilon_{\text{diel}} = 5$) sandwiched between two anisotropic WS slabs. Linear polarizers are represented by silver grids, while wavy curves depict the electric fields of linearly polarized waves moving in the $+z$ and $-z$ directions. The $+z$ direction is along the separation of Weyl nodes in momentum space **b**. Matrices $\overline{\overline{M}}_{+90} = 90°$ and $\overline{\overline{M}}_{-45} = -45°$ stand for the Jones matrices of the two polarizers. Rotation tuning is achieved by rotating the rightmost WS layer by an angle Ψ. (b) and (c) Asymmetry $\Delta T = |T_{+z}|^2 - |T_{-z}|^2$ and isolation $I = 10\lg\left(|T_{+z}|^2/|T_{-z}|^2\right)$ as a function of frequency and thickness of the WS for $\Psi = 0°$. $|T_{+z}|^2$ ($|T_{-z}|^2$) is the sum of transmission of all polarization components, including the cross-polarisation, $|T_{+z}|^2 = \sum_{\substack{i=x,y \\ j=x,y}} |T_{+z}^{ij}|^2$ in the $+z$ ($-z$) direction.

through, effectively achieving the one-way transmission of light.

Upon a comprehensive examination of existing theoretical and experimental research on the optical characteristics of WSs, we choose to utilize the relative permittivity tensor [25, 45].

$$\varepsilon_{WS} = \begin{pmatrix} \varepsilon_d & i\varepsilon_a & 0 \\ -i\varepsilon_a & \varepsilon'_d & 0 \\ 0 & 0 & \varepsilon_d \end{pmatrix}. \quad (1)$$

and unity magnetic permeability. The Weyl nodes splitting in momentum space by the vector $\mathbf{b}$ gives rise to the off-diagonal components $\varepsilon_a = be^2/2\pi^2\hbar\omega$ enabling the nonreciprocal behavior. As a result, WSs support magneto-optical effects when light propagates along this vector ($\mathbf{k}\|\mathbf{b}$), where $\mathbf{k}$ denotes the light wave vector. In our study, we utilize the Weyl semimetal $EuCd_2As_2$ [46, 47] that possesses the relative permittivity tensor (1) [23]. In this semimetal, the electric permittivity exhibits the characteristics of axion electrodynamics [45]. Importantly, our analysis can encompass other types of Weyl semimetals. To determine the diagonal components, we employ the Kubo–Greenwood formalism [45, 48]. Remarkably, ε_a and ε_d exhibit values on the order of unity across the entire spectrum, indicating an exceptionally large magneto-optical parameter $\varepsilon_a/\varepsilon_d \approx 1$. This result significantly improves over conventional magneto-optical materials in IR [27, 28]. Further details can be found in the Supplementary material (SM). Our model utilizes parameters close to experimental values, as presented in ref. [25] and Supplementary material.

We introduce the anisotropy in the diagonal terms of the tensor by $\varepsilon'_d \neq \varepsilon_d$. Figure S1 in Supplementary material illustrates the frequency dispersion of the real part of the ε_d, ε_a, and ε'_d. Anisotropy is invoked by shifting the plasma frequency for the y-component of the dielectric tensor [49, 50]. For example, the in-plane optical anisotropy can be intrinsic in noncentrosymmetric WS [43, 44]. Another way to in-plane anisotropy involves creating corrugations with subwavelength granularity to achieve an anisotropic effective permittivity. This approach has been recently implemented in developing hyperbolic metasurfaces [49]. We describe this approach, and its results in Figure 4. The in-plane anisotropy of the material presents a compelling opportunity to exert control over the optical response by manipulating the relative orientation of its layers. This concept has been recently explored in anisotropic metasurfaces and natural materials [51–55]. In our structures, the rotation tuning is achieved by rotating the rightmost WS layer by angle Ψ.

The calculation of transmission coefficients is carried out using the generalized T-matrix formalism [56–58] and reinforced by rigorous full-wave numerical simulations. The generalized matrix formalism [57] allows the calculation of light transmission in an isotropic or anisotropic medium for any number of layers. This algorithm is numerically stable and gives continuous solutions. We compute a transfer matrix that includes transmission coefficients for x- and y-polarized light. Jones matrices are utilized to account for the linear polarizers. The thickness of the dielectric $h_{\text{diel}} = 0.85$ μm enables the Fabry–Perot mode at the plasma frequency of WS ($\text{Re}(\varepsilon_d) = 0$), $\Omega_p = 4.2 \times 10^{14}$ rad/s. The thickness of the WSs $h_W = 0.37$ μm was optimized to ensure maximum asymmetry $\Delta T = |T_{+z}|^2 - |T_{-z}|^2$ and isolation $I = 10\lg\left(|T_{+z}|^2/|T_{-z}|^2\right)$, Figure 1(b) and (c). Here, $|T_{+z}|^2$ ($|T_{-z}|^2$) is the sum of the transmission of all polarization components, including the cross-polarisation, $|T_{+z}|^2 = \sum_{\substack{i=x,y \\ j=x,y}} |T^{ij}_{+z}|^2$ in the $+z$ ($-z$) direction. The maximum isolation for selected optimized parameters reaches 54 dB at the frequency $\omega = 5.4 \times 10^{14}$ rad/s ($\lambda = 3.5$ μm), Figure 1(c). The total length of the structure without polarizers is $L = 1.59$ μm, which is only 0.45λ at the maximum isolation.

Figure 2(a) and (b) show the forward ($+z$) and backward ($-z$) transmittance of the structure as a function of the rotation angle between the layers and frequency. The system exhibits excellent isolation properties with the complete transmission in the forward direction and vanishing transmission in the backward direction. The results of the isolation spectrum are shown in Figure 2(c). The isolation is tuned by adjusting the rotation angle, reaching a maximum of 60 dB at $\Psi = 38°$ and $\omega = 4.9 \times 10^{14}$ rad/s ($\lambda = 3.8$ μm), Figure 2(d). This excellent isolation occurs for a remarkably thin isolator of length $L = 0.45\lambda$. The relative rotation of the WS layers changes the amplitude and frequency of the isolation, providing a unique approach to tunable optical isolators, Figure 2(c) and (d).

Now we demonstrate that the anisotropy of WSs in this geometry can operate as a polarizer, eliminating the $-45°$ polarizer and making the design even more compact. Figure 3(a) shows the geometry of the proposed compact isolator with only one input polarization beam splitter. The thickness of the first layer of the WS is adjusted to $h_W = 0.92$ μm to reach maximum isolation of 20 dB at $\omega = 3 \times 10^{14}$ rad/s (the plasma frequency for ε'_a) and the twisting angle $\Psi = 50°$, Figure 3(b). While the lack of a polarizer requires the first layer of the WS to be thicker to achieve high isolation, the design can be thinner in practice because polarizers are typically positioned several

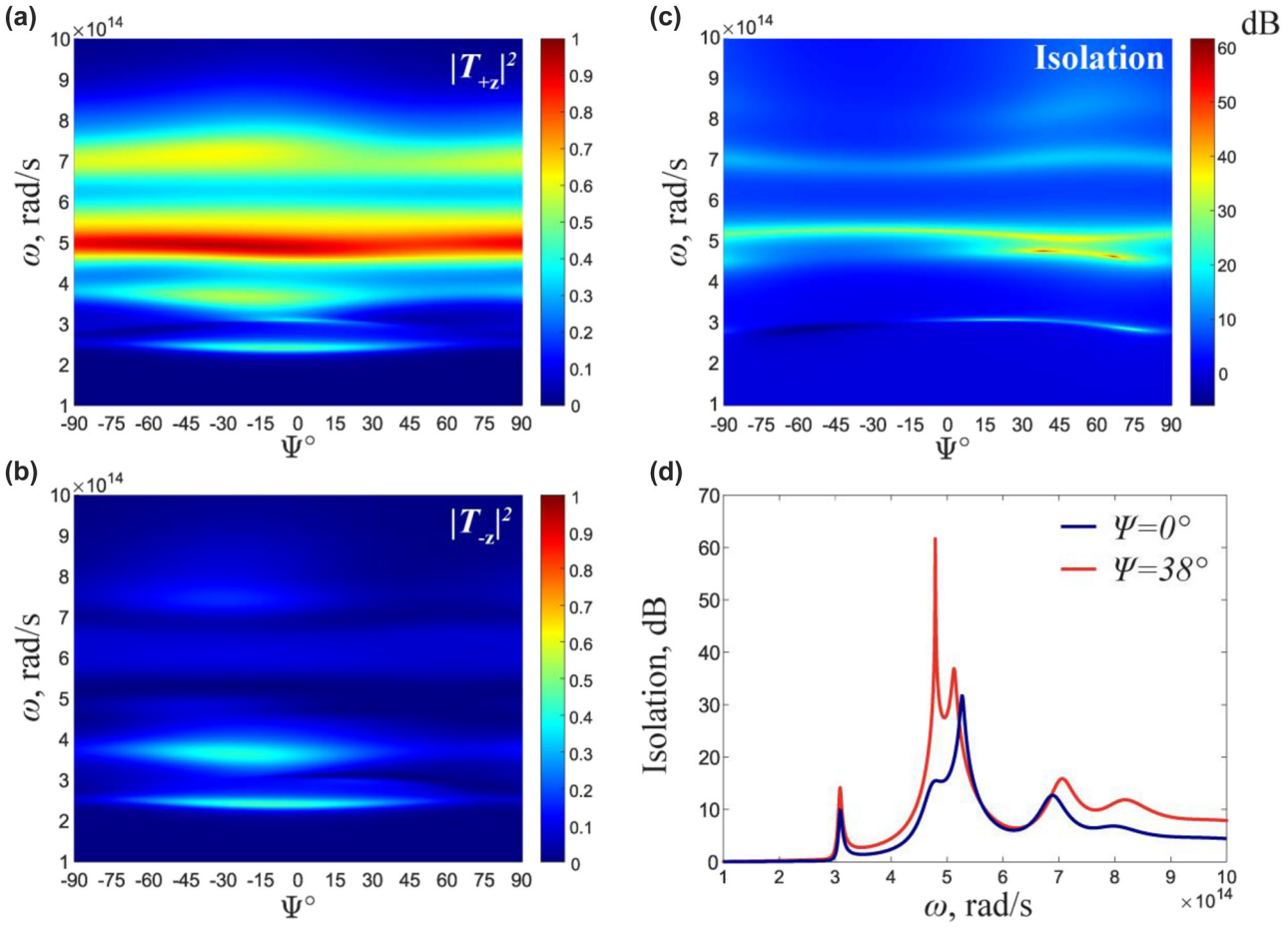

Figure 2: Tunability of Isolation coefficient. (a) and (b) Transmittance as a function of frequency ω and rotation angle Ψ in $+z$ and $-z$ directions, respectively. (c) Isolation versus frequency and rotation angle. (d) Isolation coefficient $I = 10\lg\left(|T_{+z}|^2/|T_{-z}|^2\right)$ as a function of frequency at the twist angle 0° and 38°.

wavelengths away from the structure. Other geometrical parameters are the same as in Figures 1 and 2. Figure 3(c) shows the isolation spectrum as a function of the relative rotation and frequency. At the plasma frequency $\omega = 3 \times 10^{14}$ rad/s of the anisotropic component ε_d', an isolation resonance arises, which is tuned with rotation, reaching an extreme at the twisting angle $\Psi = \pm 50°$ where the isolation reaches ± 20 dB, Figure 3(d). Therefore, at this rotation angle, the maximum effect is achieved when the polarization of the backward wave turns into a horizontal one and is blocked by the incoming polarizer. This design allows for both spectral control of isolation and the ability to control its direction, including the reversal of isolation.

Next, we examine how the anisotropy of WSs can be attained by incorporating periodic corrugations of the WSs' surface, as depicted in Figure 4(a). Here the grooves in the corrugated slabs are solely responsible for the anisotropy. The effective plasma frequency of the Weyl semimetal with surface corrugation can be controlled by adjusting the period and height of the corrugated surface. We validate our analytical results through full-wave simulations using CST Microwave Studio, where unit-cell boundary conditions and Floquet's ports simulate the periodic structure. To achieve a metasurface regime, we select a corrugation width a at least 10 times smaller than the wavelength at the resonant plasma frequency $\Omega_p = 4.2 \times 10^{14}$ rad/s. We choose $a = 0.11$ μm, with a depth of $t = 0.47$ μm and $p = 0.14$ μm. To achieve higher isolation, we adjust the thickness of the WS in simulations to $h_W = 0.7$ μm resulting in a total isolator thickness of $L = 2.34$ μm. Figure 4(c) depicts the $|E_x|^2$ distribution in the yz-plane for the structure with a relative twist angle of $\Psi = 0°$ and frequency $\omega = 2.7 \times 10^{14}$ rad/s. As expected from our analytical analysis, this scenario is reciprocal and symmetric, $\Delta T = |T_{+z}^{xx}|^2 - |T_{-z}^{xx}|^2 = 0$. In Figure 4(d), we present the $|E_x|^2$ field distribution at a relative twist angle $\Psi = 90°$. The figure reveals that the structure transmits x polarisation of radiation ($|T_{+z}^{xx}|^2$) in $+z$, while almost entirely suppressing it in the opposite

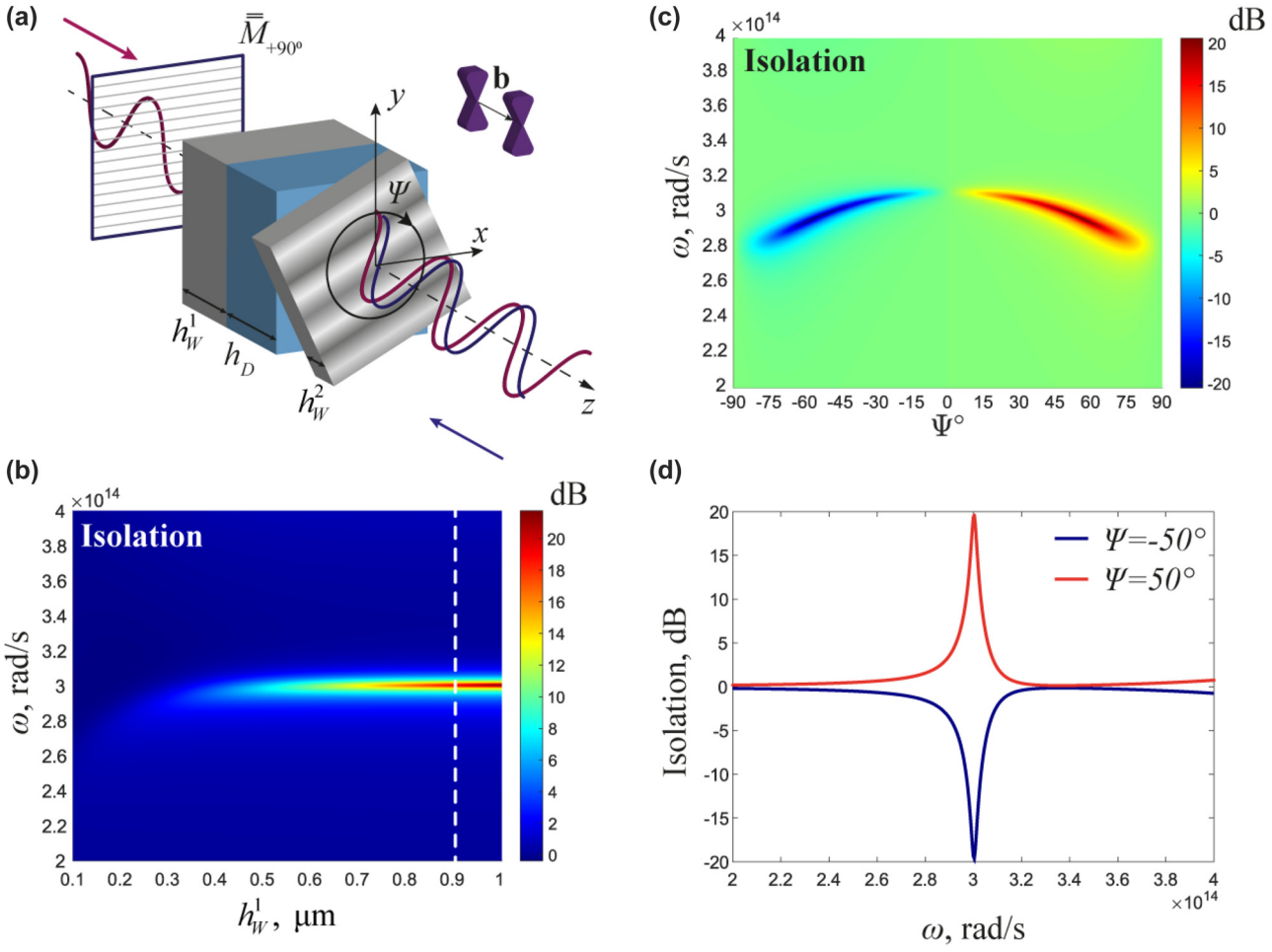

Figure 3: Optical isolation with one polarizer. (a) Isolator geometry with one polarizer. (b) Isolation spectrum $I = 10\lg\left(|T_{+z}|^2/|T_{-z}|^2\right)$ as a function of frequency and thickness of the Weyl semimetal at a rotation angle $\Psi = 50°$. (c) Isolation as a function of frequency and angle of rotation. (d) Isolation coefficient $I = 10\lg\left(|T_{+z}|^2/|T_{-z}|^2\right)$ as a function of frequency at the twist angle $-50°$ and $50°$.

direction ($|T_{-z}^{xx}|^2 \approx 0$). The asymmetry coefficient obtained reaches 85 % at $\omega = 2.7 \times 10^{14}$ rad/s ($L = 3.9$ μm), in good agreement with the analytical results, Figure 4(b). We note a slight discrepancy between the CST simulation and T-matrix analytical results. This discrepancy arises because, in the CST simulation, the plasma frequency shift is specified by applying a corrugated surface, which does not perfectly align with the permittivity tensor in the analytical model.

The current design is a Faraday rotator that works as a polarized isolator, exhibiting significant isolation solely for specific polarizations of forward and backward waves. Without polarizers enabling polarization selection, waves with arbitrary incoming polarization cannot be blocked entirely. Nonetheless, this limitation can be overcome by increasing the thicknesses of the anisotropic WS layers or using at least one polarizer.

Regarding potential fabrication approaches for the discussed structures, bulk single crystals of $EuCd_2As_2$ can be grown by the NaCl/KCl flux method [46, 59]. Subsequently, surface corrugation can be introduced on the crystal surface using advanced nanofabrication techniques, such as electron beam lithography (EBL), nanoimprint lithography (NIL), focused ion beam (FIB) milling, reactive ion etching (RIE) or cleaving from the bulk crystals as recently demonstrated for Weyl semimetal WTe_2 [22].

Lastly, we discuss the tunability mechanism of our proposed isolator. This key attribute is rooted in the anisotropy within the permittivity tensor, an effect of the corrugated structure in the Weyl semimetal layers. Through this electromagnetic feature, we can control the overlap of spatial profiles of intrinsic photonic modes in each slab, ultimately modulating the far-field properties, reflections and transmissions. This tuning method, derived from recent studies

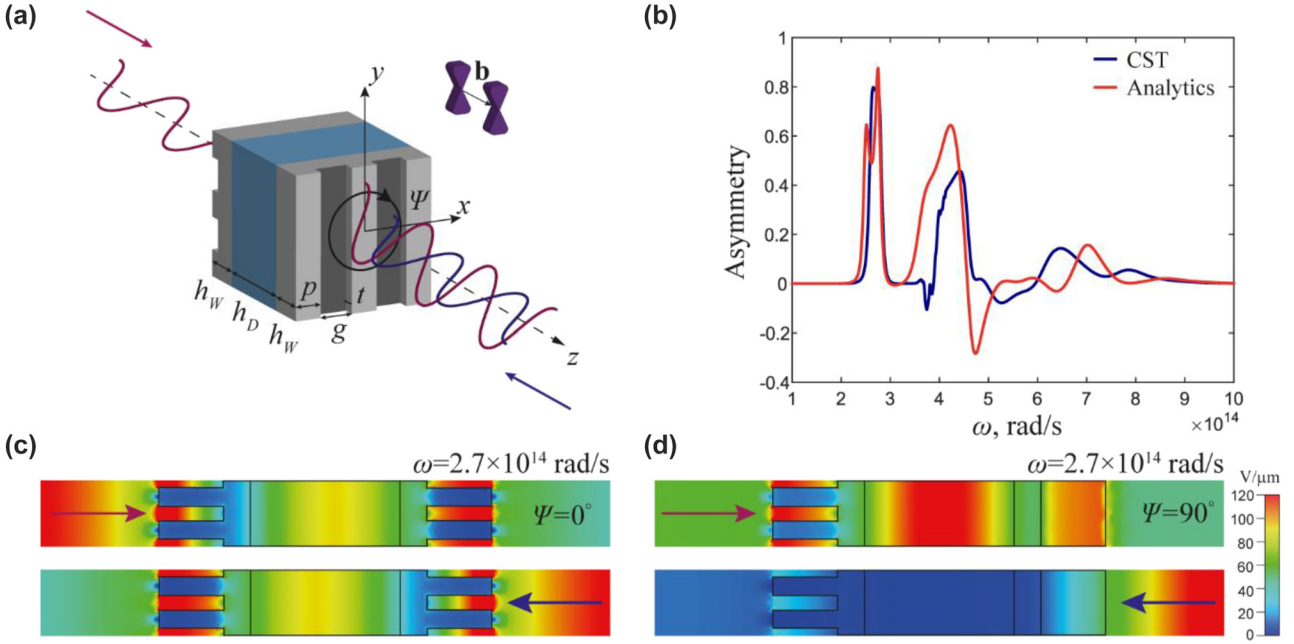

Figure 4: Optical isolation with corrugated Weyl semimetals. (a) Faraday rotator geometry with corrugated metasurface surface and without polarizers. (b) Transmittance asymmetry $\Delta T = |T^{xx}_{+z}|^2 - |T^{xx}_{-z}|^2$ as a function of frequency at the twist angle $\Psi = 90°$. The analytical results are obtained using the *T*-matrix approach with the effective material parameters for the corrugated metasurfaces extracted from full-wave simulations in CST microwave studio. (c) and (d) Absolute value of $|E_x|^2$ distribution of the isolator in the *yz*-plane at the twist angle (a) $\Psi = 0°$ and (c) $\Psi = 90°$ and frequency $\omega = 2.7 \times 10^{14}$ rad/s, for the forward (upper) and backward (lower) propagation.

on polariton manipulation in similar systems [55, 60], grants our design flexibility in operation.

3 Conclusions

This work presents a novel approach to tunable optical isolation based on twisted bilayered Weyl semimetals. We have demonstrated that our approach has enabled highly efficient tuning of both direction and value of isolation by utilizing the relative rotation of bilayered Weyl semimetals. The structure of the Faraday isolator with two polarizers consists of two anisotropic Weyl semimetals layers separated by a dielectric. We have shown that this approach has achieved isolation exceeding 50 dB and an insertion loss as small as 0.33 dB. Moreover, we have found that the anisotropy of the Weyl semimetals has made it possible to eliminate one of the polarizers in the isolator, simplifying the model and making it more compact. The tunable properties, high isolation coefficient, and the absence of a requirement for an external magnetic field and ultrasmall sizes make our proposed design superior to other approaches based on magneto-optical or temporal modulation effects. We anticipate that further development of Weyl semimetals and reducing their material losses will lead to even better performance characteristics of these optical isolators.

Author contributions: All authors have accepted responsibility for the entire content of this manuscript and approved its submission. All the authors discussed the results.
Research funding: Alex Krasnok thanks the ECE department of Florida International University. S.F., A.A. acknowledge support from the AFOSR MURI program.
Conflict of interest statement: Authors state no conflicts of interest.
Informed consent: Informed consent was obtained from all individuals included in this study.
Ethical approval: The conducted research is not related to either human or animal use.
Data availability: The datasets generated and/or analyzed during the current study are available from the corresponding author upon reasonable request.

References

[1] N. Morali, R. Batabyal, P. K. Nag, et al., “Fermi-Arc diversity on surface terminations of the magnetic Weyl semimetal Co 3 Sn 2 S 2,” *Science*, vol. 365, p. 1286, 2019.

[2] M. M. Otrokov, I. P. Rusinov, M. Blanco-Rey, et al., "Unique thickness-dependent properties of the van Der waals interlayer antiferromagnet MnBi2Te4," *Phys. Rev. Lett.*, vol. 122, p. 107202, 2019.
[3] N. P. Armitage, "Constraints on Jones transmission matrices from time-reversal invariance and discrete spatial symmetries," *Phys. Rev. B*, vol. 90, p. 035135, 2014.
[4] X. Ni, S. Yves, A. Krasnok, and A. Alu, "Topological metamaterials," ArXiv Prepr. arXiv:2211, 2023.
[5] K. Kuroda, T. Tomita, M. T. Suzuki, et al., "Evidence for magnetic Weyl fermions in a correlated metal," *Nat. Mater.*, vol. 16, p. 1090, 2017.
[6] I. Belopolski, K. Manna, D. S. Sanchez, et al., "Discovery of topological Weyl fermion lines and drumhead surface states in a room temperature magnet," *Science*, vol. 365, p. 1278, 2019.
[7] X. Wan, A. M. Turner, A. Vishwanath, and S. Y. Savrasov, "Topological semimetal and fermi-arc surface states in the electronic structure of pyrochlore iridates," *Phys. Rev. B*, vol. 83, p. 205101, 2011.
[8] A. A. Burkov and L. Balents, "Weyl semimetal in a topological insulator multilayer," *Phys. Rev. Lett.*, vol. 107, p. 127205, 2011.
[9] S.-Y. Xu, I. Belopolski, N. Alidoust, et al., "Discovery of a Weyl fermion semimetal and topological fermi arcs," *Science*, vol. 349, p. 613, 2015.
[10] S.-Y. Xu, I. Belopolski, D. S. Sanchez, et al., "Experimental discovery of a topological Weyl semimetal state in TaP," *Sci. Adv.*, vol. 1, p. 031013, 2015.
[11] K. Y. Yang, Y. M. Lu, and Y. Ran, "Quantum Hall effects in a Weyl semimetal: possible application in pyrochlore iridates," *Phys. Rev. B*, vol. 84, p. 075129, 2011.
[12] A. A. Soluyanov, D. Gresch, Z. Wang, et al., "Type-II Weyl semimetals," *Nature*, vol. 527, p. 495, 2015.
[13] S. Murakami, "Phase transition between the quantum spin Hall and insulator phases in 3D: emergence of a topological gapless phase," *New J. Phys.*, vol. 9, p. 356, 2007.
[14] L. Lu, Z. Wang, D. Ye, et al., "Experimental observation of Weyl points," *Science*, vol. 349, p. 622, 2015.
[15] L. Lu, J. D. Joannopoulos, and M. Soljačić, "Topological photonics," *Nat. Photonics*, vol. 8, p. 821, 2014.
[16] W. Gao, M. Lawrence, B. Yang, et al., "Topological photonic phase in chiral hyperbolic metamaterials," *Phys. Rev. Lett.*, vol. 114, p. 037402, 2015.
[17] B. Yang, Q. Guo, B. Tremain, et al., "Ideal Weyl points and helicoid surface states in artificial photonic crystal structures," *Science*, vol. 359, p. 1013, 2018.
[18] B. Yang, Q. Guo, B. Tremain, et al., "Direct observation of topological surface-state arcs in photonic metamaterials," *Nat. Commun.*, vol. 8, p. 97, 2017.
[19] W. Gao, B. Yang, M. Lawrence, F. Fang, B. Béri, and S. Zhang, "Photonic Weyl degeneracies in magnetized plasma," *Nat. Commun.*, vol. 7, p. 12435, 2016.
[20] A. A. Burkov, "Anomalous Hall effect in Weyl metals," *Phys. Rev. Lett.*, vol. 113, p. 187202, 2014.
[21] S. Zhong, J. E. Moore, and I. Souza, "Gyrotropic magnetic effect and the magnetic moment on the fermi surface," *Phys. Rev. Lett.*, vol. 116, p. 077201, 2016.
[22] C. Tan, Z. Yue, Z. Dai, et al., "Nanograting-assisted generation of surface plasmon polaritons in Weyl semimetal WTe2," *Opt. Mater.*, vol. 86, p. 421, 2018.
[23] V. S. Asadchy, C. Guo, B. Zhao, and S. Fan, "Sub-wavelength passive optical isolators using photonic structures based on Weyl semimetals," *Adv. Opt. Mater.*, vol. 8, p. 2000100, 2020.
[24] Y. Tsurimaki, X. Qian, S. Pajovic, F. Han, M. Li, and G. Chen, "Large nonreciprocal absorption and emission of radiation in type-I Weyl semimetals with time reversal symmetry breaking," *Phys. Rev. B*, vol. 101, p. 165426, 2020.
[25] O. V. Kotov and Y. E. Lozovik, "Giant tunable nonreciprocity of light in Weyl semimetals," *Phys. Rev. B*, vol. 98, p. 195446, 2018.
[26] B. Zhao, C. Guo, C. A. C. Garcia, P. Narang, and S. Fan, "Axion-field-enabled nonreciprocal thermal radiation in Weyl semimetals," *Nano Lett.*, vol. 20, p. 1923, 2020.
[27] C. Guo, V. S. Asadchy, B. Zhao, and S. Fan, "Light control with Weyl semimetals," *ELight*, vol. 3, p. 2, 2023.
[28] V. S. Asadchy, M. S. Mirmoosa, A. Diaz-Rubio, S. Fan, and S. A. Tretyakov, "Tutorial on electromagnetic nonreciprocity and its origins," *Proc. IEEE*, vol. 108, p. 1684, 2020.
[29] D. Jalas, A. Petrov, M. Eich, et al., "What is-and what is not-an optical isolator," *Nat. Photonics*, vol. 7, p. 579, 2013.
[30] C. Caloz, A. Alù, S. Tretyakov, D. Sounas, K. Achouri, and Z.-L. Deck-Léger, "Electromagnetic nonreciprocity," *Phys. Rev. Appl.*, vol. 10, p. 047001, 2018.
[31] G. Fürnkranz, *The Quantum Internet*, Cham, Springer International Publishing, 2020.
[32] H. J. Kimble, "The quantum internet," *Nature*, vol. 453, p. 1023, 2008.
[33] S. V. Kutsaev, A. Krasnok, S. N. Romanenko, A. Y. Smirnov, K. Taletski, and V. P. Yakovlev, "Up-and-coming advances in optical and Microwave nonreciprocity: from classical to quantum realm," *Adv. Photonics Res.*, vol. 2, p. 2000104, 2021.
[34] A. Krasnok and A. Alù, "Low-symmetry nanophotonics," *ACS Photonics*, vol. 9, p. 2, 2022.
[35] A. B. Khanikaev and M. J. Steel, "Low-symmetry magnetic photonic crystals for nonreciprocal and unidirectional devices," *Opt. Express*, vol. 17, p. 5265, 2009.
[36] A. Figotin and I. Vitebsky, "Nonreciprocal magnetic photonic crystals," *Phys. Rev. E: Stat., Nonlinear, Soft Matter Phys.*, vol. 63, p. 1, 2001.
[37] A. C. Mahoney, J. I. Colless, S. J. Pauka, et al., "On-chip Microwave quantum Hall circulator," *Phys. Rev. X*, vol. 7, p. 011007, 2017.
[38] Z. Yu and S. Fan, "Complete optical isolation created by indirect interband photonic transitions," *Nat. Photonics*, vol. 3, p. 91, 2009.
[39] C. Zhao, G. Hu, Y. Chen, Q. Zhang, Y. Zhang, and C.-W. Qiu, "Unidirectional bound states in the continuum in Weyl semimetal nanostructures," *Photonics Res.*, vol. 10, p. 1828, 2022.
[40] J. Wu, Y. Xiang, and X. Dai, "Tunable broadband compact optical isolator based on Weyl semimetal," *Results Phys.*, vol. 46, p. 106290, 2023.
[41] N. P. Armitage, E. J. Mele, and A. Vishwanath, "Weyl and Dirac semimetals in three-dimensional solids," *Rev. Mod. Phys.*, vol. 90, p. 015001, 2018.
[42] X. Han, A. Markou, J. Stensberg, Y. Sun, C. Felser, and L. Wu, "Giant intrinsic anomalous terahertz Faraday rotation in the magnetic Weyl semimetal Co2MnGa at room temperature," *Phys. Rev. B*, vol. 105, p. 174406, 2022.
[43] Y. Liu, Q. Gu, Y. Peng, et al., "Raman signatures of broken inversion symmetry and in-plane anisotropy in type-II Weyl semimetal candidate TaIrTe 4," *Adv. Mater.*, vol. 30, p. 1706402, 2018.

[44] R. Zu, M. Gu, L. Min, et al., "Comprehensive anisotropic linear optical properties of the Weyl semimetals TaAs and NbAs," *Phys. Rev. B*, vol. 103, p. 165137, 2021.
[45] J. Hofmann and S. Das Sarma, "Surface plasmon polaritons in topological Weyl semimetals," *Phys. Rev. B*, vol. 93, p. 241402, 2016.
[46] J.-R. Soh, F. de Juan, M. G. Vergniory, et al., "Ideal Weyl semimetal induced by magnetic exchange," *Phys. Rev. B*, vol. 100, p. 201102, 2019.
[47] J. Ma, H. Wang, S. Nie, et al., "Emergence of nontrivial low-energy Dirac fermions in antiferromagnetic EuCd 2 as 2," *Adv. Mater.*, vol. 32, p. 1907565, 2020.
[48] O. V. Kotov and Y. E. Lozovik, "Dielectric response and novel electromagnetic modes in three-dimensional Dirac semimetal films," *Phys. Rev. B*, vol. 93, p. 1, 2016.
[49] P. Li, G. Hu, I. Dolado, et al., "Collective near-field coupling and nonlocal phenomena in infrared-phononic metasurfaces for nano-light canalization," *Nat. Commun.*, vol. 11, p. 3663, 2020.
[50] D. G. Baranov, Y. Xiao, I. A. Nechepurenko, A. Krasnok, A. Alù, and M. A. Kats, "Nanophotonic engineering of far-field thermal emitters," *Nat. Mater.*, vol. 18, p. 920, 2019.
[51] Y. Chen, H.-X. Wang, Q. Bao, J.-H. Jiang, and H. Chen, "Ideal type-II Weyl points in twisted one-dimensional dielectric photonic crystals," *Opt. Express*, vol. 29, p. 40606, 2021.
[52] J. Peng, G. Tang, L. Wang, R. Macêdo, H. Chen, and J. Ren, "Twist-induced near-field thermal switch using nonreciprocal surface magnon-polaritons," *ACS Photonics*, vol. 8, p. 2183, 2021.
[53] S. Mukherjee, J. Gomis-Bresco, P. Pujol-Closa, D. Artigas, and L. Torner, "Angular control of anisotropy-induced bound states in the continuum," *Opt. Lett.*, vol. 44, p. 5362, 2019.
[54] G. Tang, J. Chen, and L. Zhang, "Twist-induced control of near-field heat radiation between magnetic Weyl semimetals," *ACS Photonics*, vol. 8, p. 443, 2021.
[55] G. Hu, Q. Ou, G. Si, et al., "Topological polaritons and photonic magic angles in twisted α-MoO3 bilayers," *Nature*, vol. 582, p. 209, 2020.
[56] N. C. Passler, M. Jeannin, and A. Paarmann, "Layer-resolved absorption of light in arbitrarily anisotropic heterostructures," *Phys. Rev. B*, vol. 101, p. 165425, 2020.
[57] N. C. Passler and A. Paarmann, "Generalized 4 × 4 matrix formalism for light propagation in anisotropic stratified media: study of surface phonon polaritons in polar dielectric heterostructures," *J. Opt. Soc. Am. B*, vol. 34, p. 2128, 2017.
[58] D. W. Berreman, "Optics in stratified and anisotropic media: 4×4-matrix formulation," *J. Opt. Soc. Am.*, vol. 62, p. 502, 1972.
[59] I. Schellenberg, U. Pfannenschmidt, M. Eul, C. Schwickert, and R. Pöttgen, "A 121Sb and 151Eu mössbauer spectroscopic investigation of EuCd2X2 (X = P, as, Sb) and YbCd2Sb2," *Z. Anorg. Allg. Chem.*, vol. 637, p. 1863, 2011.
[60] G. Hu, A. Krasnok, Y. Mazor, C. Qiu, and A. Alù, "Moiré hyperbolic metasurfaces," *Nano Lett.*, vol. 20, p. 3217, 2020.

Supplementary Material: This article contains supplementary material (https://doi.org/10.1515/nanoph-2023-0241).